

# Generation of bright circularly-polarized extreme ultraviolet high harmonics for magnetic circular dichroism spectroscopy

Ofer Kfir<sup>1</sup>, Patrik Grychtol<sup>2</sup>, Emrah Turgut<sup>2</sup>, Ronny Knut<sup>2,3</sup>, Dmitriy Zusin<sup>2</sup>,  
Dimitar Popmintchev<sup>2</sup>, Tenio Popmintchev<sup>2</sup>, Hans Nembach<sup>3</sup>, Justin M. Shaw<sup>3</sup>, Avner Fleischer<sup>1,4</sup>,  
Henry Kapteyn<sup>2</sup>, Margaret Murnane<sup>2</sup> and Oren Cohen<sup>1</sup>.

<sup>1</sup>*Solid State Institute and Physics Department, Technion, Haifa 32000, Israel*

<sup>2</sup>*Department of Physics and JILA, University of Colorado and NIST, Boulder, CO 80309, USA*

<sup>3</sup>*Electromagnetics Division, National Institute of Standards and Technology, Boulder, CO 80305, USA*

<sup>4</sup>*Department of Physics and Optical Engineering, Ort Braude College, Karmiel 21982, Israel*

Corresponding authors: [ofertx@technion.ac.il](mailto:ofertx@technion.ac.il), [oren@technion.ac.il](mailto:oren@technion.ac.il)

Circularly-polarized extreme UV and X-ray radiation provides valuable access to the structural, electronic and magnetic properties of materials. To date, such experiments have been possible only using large-scale free-electron lasers or synchrotrons. Here we demonstrate the first bright extreme UV circularly-polarized high harmonics and use this new light source for magnetic circular dichroism measurements at the *M*-shell absorption edges of cobalt. This work paves the way towards element-specific imaging and spectroscopy of multiple elements simultaneously in magnetic and other chiral media with very high spatio-temporal resolution, all on a tabletop.

## Introduction

Circularly polarized radiation in the extreme ultraviolet (EUV) and soft X-ray spectral regions has proven to be extremely useful for investigations of chirality-sensitive light-matter interactions and other phenomena. These include circular dichroism of photoelectrons from chiral molecules [1], ultrafast molecular decay dynamics [2], direct measurement of quantum phases (*e.g.* Berry's phase and pseudo-spin) in graphene and topological insulators [3–5] and reconstruction of band structure and modal phases in solids [6]. With regard to magnetic materials, circularly polarized soft x-rays are particularly useful for X-ray Magnetic Circular Dichroism (XMCD) spectroscopy [7]. XMCD allows for element-selective probing as well as coherent imaging and holography of magnetic structures with nanometer resolution [8–10]. Moreover, it can be used to extract detailed information about the magnetic state by distinguishing between the spin and orbital magnetic moments of each element. Thus, time resolved XMCD can probe the element-specific dynamics of the spin and orbit moments when interacting with the electronic and phononic degrees of freedom in a material [11–14]. However, the time resolution available to date for XMCD has been  $> 100$  fs, limited by the pulse duration and jitter of synchrotron pulses [15–17]. Moreover, it has not been possible to probe spin dynamics of multiple elements simultaneously within the same sample, because the photon energy must be tuned across the various absorption edges.

Table-top soft x-ray sources based on high harmonic upconversion of femtosecond laser pulses represent a viable alternative to large-scale sources for many applications, due to their unique

ability to generate bright, broadband, ultrashort and coherent light with an energy spectrum reaching into the keV region [18]. High harmonic generation (HHG) not only enables coherent imaging of nanometer structures with a spatial resolution approaching the diffraction limit [19], but also accesses the fastest dynamics in atoms, molecules, solids and plasmas with unprecedented time resolution [20–26]. The large bandwidth and short temporal duration of HHG makes it a versatile, element-specific probe of coupled spin, charge and phonon dynamics on ultrafast timescales. In the case of magnetic materials, recent work has shown that HHG can simultaneously probe the magnetic state of the 3d ferromagnets Fe, Co and Ni, by taking advantage of the fact that the reflectivity near the M-shell absorption edges depends on the orientation as well as the magnitude of the magnetization [27,28]. This novel capability made it possible to uncover new fundamental understanding about the timescale of the exchange interaction, as well as local spin scattering and non-local spin transport, all of which can occur on few-femtosecond timescales [29–31]. The vast majority of HHG applications to date, however, used linearly polarized light that can be generated relatively efficiently.

For decades it was assumed that high harmonic generation from atoms was brightest when both the driving laser and HHG fields were linearly polarized. The source for this misconception is that HHG is a recollision phenomenon. A bound electron is ripped off the atom by the intense electric field of the driving laser pulse and then accelerated in the continuum until it undergoes a coherent recollision with its parent ion [32,33]. For a linearly polarized driving field, the electron accelerates on a linear trajectory - and therefore easily recollides with the parent ion. When driven by an elliptical laser field with a small degree of ellipticity, the electron has some probability to recollide with its parent ion due to lateral spreading (quantum diffusion) of the wavefunction in the continuum [34,35]. This results in the generation of slightly elliptically polarized high harmonics [36,37]. In contrast, for circularly-polarized driving lasers (or elliptically-polarized laser with a large ellipticity), the probability for recollision and emission of high harmonics is completely suppressed. Nevertheless, because of important applications in materials science, there was strong motivation to generate bright circularly polarized high harmonic beams [38–47]. The first experimentally measured circularly polarized high-order harmonics were produced by converting the polarization of linearly polarized HHG to circular, by using a reflective quarter-waveplate [44]. This approach is very lossy, is limited to narrow spectral regions constrained by available multilayer mirror materials, and to date has not been employed for applications. A direct approach for generating circularly-polarized HHG was suggested almost two decades ago [48,49] and recently measured by Fleischer *et al.* [50]. In this scheme, circularly polarized high harmonics are driven by co-propagating circularly-polarized bi-chromatic fields that rotate in opposite directions and interact with an isotropic gas. Notably, Fleischer *et al.* measured the ellipticity of the harmonics, but not their helicity.

In this work, we generate bright circularly-polarized high harmonic beams for the first time, and then use this unique tabletop light source to implement the first magnetic circular dichroism

measurements of magnetic materials. We generate bright circularly-polarized high harmonics by co-propagating bi-chromatic driving lasers (Ti:Sapphire fundamental and the second harmonic beams) that are circularly-polarized with opposite helicity in a gas-filled hollow waveguide. Using Neon gas, we extend the circularly-polarized high harmonics spectrum to the M-edges of 3d ferromagnets, and maximize the brightness of our source by optimizing the gas pressure. Finally, we measured the circular dichroism of Cobalt throughout the M-shell absorption edge spectral region. This measurement is also the first to measure the helicity of the circularly polarized high-order harmonic beams. In the future, the use of mid-infrared pump lasers should make it possible to generate bright circularly-polarized high-harmonics at the L-shell absorption edges of ferromagnets, slightly below 1 keV [18].

### **Bright circularly-polarized high harmonics**

We generate bright circularly polarized harmonics by co-propagating bi-chromatic 790 nm and 395 nm ( $\omega$  and  $2\omega$ ) driving laser beams with counter-rotating circular polarization [48–50]. This approach has several properties that are beneficial for applications. First, the conversion efficiency to circularly polarized high harmonics is comparable to the conversion efficiency of traditional HHG, where linearly polarized driving lasers produce linearly polarized high harmonics (see Fig. S.2 in Ref. 50). Second, the generated spectrum consists only of circularly polarized harmonics. Third, consecutive harmonics exhibit opposite helicity. Fourth, the circular-polarization of the harmonics is directly manifested in the high harmonic spectrum: thus, it is not essential to directly or continuously monitor their polarization. As explained below, when the bi-chromatic driving lasers consist of the fundamental and second harmonic frequencies, very reduced intensities of every  $3k^{\text{th}}$  ( $k=1,2,3\dots$ ) harmonic indicate that the polarizations of  $3k+1$  and  $3k-1$  harmonics are circular with helicity that correspond to the polarization of the fundamental and  $2^{\text{nd}}$  harmonic fields, respectively. Fifth, the polarization of the generated harmonics is largely insensitive to the intensities and intensity ratio between the bi-chromatic driving lasers. This is an important feature because the intensities (and the intensity ratio) can vary transversally within the focal spot and along the direction of propagation. Also, this feature is important for the robustness of the method to misalignment and instability of the driving fields. Finally, the mechanism for producing circularly polarized harmonics in this direct approach is based only on the circular polarization of the driving pulses and it is otherwise insensitive with respect to the nonlinear medium and other properties of the driving lasers. Thus, we expect that many experimental applications that were implemented using linearly polarized HHG can be directly transferred to circularly polarized harmonics. For example, we expect that the use of long-wavelength bi-chromatic driving lasers will extend bright circularly-polarized HHG into the keV region, which will span the water-window region as well as the magnetically sensitive *L*-shell absorption edges of the 3d ferromagnets [18].

We first describe the theoretical spectral and polarization features of our source driven by a left circularly-polarized fundamental beam at a central wavelength of 790 nm, and a right circularly-

polarized second harmonic beam (Fig. 1a). We consider an idealized case in which the medium is isotropic and time-independent and the driving laser is perfectly periodic. Independent of the relative intensity between the two pump fields, the bi-chromatic field,  $\vec{E}_{BC}(t)$ , exhibits the following dynamical symmetry  $\vec{E}_{BC}(t + T/3) = \hat{R}_{(120^\circ)} \vec{E}_{BC}(t)$  where  $T$  is the optical cycle of the fundamental laser and  $\hat{R}_{(120^\circ)}$  is the  $120^\circ$  rotation operator in the polarization plane. The emitted HHG field conforms to the same dynamical symmetry. Thus, the complex amplitude of each  $q^{\text{th}}$ -order harmonic,  $\vec{E}_q$ , satisfies the following eigenvalue equation -

$$\vec{E}_q e^{-2\pi i q/3} = \hat{R}_{(120^\circ)} \vec{E}_q \quad (1)$$

The solutions of Eq. (1) are a left circularly-polarized field with eigenvalue  $e^{-2\pi i/3}$  and a right circularly-polarized field with eigenvalue  $e^{+2\pi i/3}$ . The left circularly-polarized  $q^{\text{th}}$ -order harmonic,  $\vec{E}_{q,L}$ , satisfies  $e^{-2\pi i/3 \cdot q} \vec{E}_{q,L} = e^{-2\pi i/3} \vec{E}_{q,L}$  which is fulfilled only when  $q=3k+1$ . Similarly, the right circularly-polarized  $q^{\text{th}}$ -order harmonic,  $\vec{E}_{q,R}$ , satisfies  $e^{-2\pi i/3 \cdot q} \vec{E}_{q,R} = e^{+2\pi i/3} \vec{E}_{q,R}$  which is fulfilled only when  $q=3k-1$ . Notably,  $q=3k$  harmonics do not satisfy Eq. (1) and are therefore theoretically forbidden, and have much reduced intensities in our experiment.

Figure 1b presents schematically the experimental setup. We use a Ti:Sapphire oscillator in combination with a single stage regenerative amplifier, delivering sub-45 fs pulses at a repetition rate of 4 kHz, which are centered at a wavelength of 790 nm (red), with an energy of 2.5 mJ per pulse. After frequency doubling the laser beam in a Beta Barium Borate (BBO) crystal, the bi-chromatic co-propagating driving fields are separated by a dichroic mirror (DM) into two different arms of a Mach-Zehnder interferometer. An optical delay stage in the red arm compensates for the relative time delay between the two colors, and the polarization of each arm is fully controlled by a set of half- and quarter-wavelength retardation plates. The red (1.6 mJ/pulse) and blue (0.43 mJ/pulse) pump lasers are focused into a 150  $\mu\text{m}$  diameter, 2 cm long gas-filled hollow waveguide using lenses with 50cm and 75cm focal lengths, respectively. The circularly polarized HHG beam emerging from the waveguide passes through an aluminum filter, to eliminate the laser light. In our first experiment, the HHG beam is then spectrally dispersed using a spectrometer composed of a toroidal mirror, a laminar gold grating with a groove density of 500 lines/mm, and a CCD camera. In our second experiment, the HHG beam passes through a magnetized 100 nm thick Cobalt foil tilted by  $45^\circ$  with respect to the harmonics beam before entering the spectrometer. The magnetization of the Cobalt foil is controlled by an external electromagnet producing approximately 60 mT parallel to the sample plane, exceeding the 20 mT coercive field of the foil. The alternating polarity of the magnet is synchronized to the read-out of the spectrometer, so that we can acquire the transmitted HHG spectrum for “up” as well as “down” magnetization. The normalized difference of these two spectra constitutes the XMCD trace. Positioning the ferromagnet sample at  $45^\circ$  degrees to the HHG beam allows observation of XMCD of an in-plane magnetized sample [51].

We first discuss the brightness, spectral and polarization features of our source. Figure 2a shows observed HHG spectrum when the fiber was filled with Argon gas at a pressure of 100 Torr, where the pump laser beams were blocked by Al filters of  $\sim 800$  nm thickness. Figure 2b displays observed HHG spectra from 650 Torr of Neon, and 70 Torr of molecular Nitrogen using 400 nm thick Aluminum filters. Clearly, the  $q=3k$  harmonics are almost completely suppressed over the entire observed HHG spectra for all gas species. This feature is a clear indication that the ellipticities of the harmonics are approximately one (*i.e.* the harmonics polarizations are close to circular) [50]. As shown in Figs. 2a-b, we detected  $\sim 10^6$  counts per second (on the CCD) in many harmonics. Figure 2c presents a pressure scan of the HHG spectra observed in Neon gas. Clearly, the  $3k$  harmonics (marked by white arrows) are suppressed throughout the entire pressure range, indicating that generation of circularly polarized HHG is robust. It is worth noting that this pressure dependent spectrogram differs from phase-matching pressure tuning scans generated by a single pump laser in hollow waveguide, in which different harmonics are brightest for different pressures [52,53]. As shown in Fig. 2c, all the harmonics are brightest for high pressures of 650 Torr. This observation suggests that the generation of circularly polarized harmonics is brightest due to propagation effects. Indeed, the current flux of circularly-polarized photons produced by our system is already sufficient for application experiments such as XMCD, as described below.

### Magnetic circular dichroism

To demonstrate that our circularly-polarized harmonics are useful for probing the magnetic state of materials and other downstream applications, we used them for measuring the dichroic magneto-optical absorption of a thin Cobalt film. The imaginary (*i.e.* absorptive) part of the refractive index,  $n$ , for light propagating in a magnetically saturated film is given by  $Im[n] = \beta \pm \Delta\beta$  where  $\beta$  is the average absorption coefficient, and  $\Delta\beta$  is the dichroic absorption coefficient for circularly polarized light, where the  $(\pm)$  marks the absorption sign change for left versus right circular polarization [51,54]. The dichroic absorption scales linearly with the component of the magnetization parallel to the light propagation direction. For example, the absorption coefficient of sample with magnetization  $M$  that is below its saturation value,  $M_{sat}$ , pointing at angle  $\theta$  with respect to the beam direction is  $(M/M_{sat}) \cos \theta \cdot \Delta\beta$ . However, XMCD requires a bright circularly polarized soft x-ray source, since the non-dichroic absorption coefficient is  $\approx 10$  times larger than the dichroic coefficient, leading to strong average absorption that far exceeds the dichroic signal.

We measured the HHG spectrum after passing through a magnetized Cobalt foil, as shown in Figs. 1 and 3. We extracted the XMCD asymmetry by flipping the magnetization of the sample. Figure 3a presents the transmitted spectrum when the foil is magnetized either “up” or “down”, labeled by  $I^{up}$  and  $I^{down}$ , respectively. The normalized XMCD asymmetry,  $A = (I^{up} - I^{down})/(I^{up} + I^{down})$  is shown in Fig. 3b. The experimental data were acquired by summing over 50 measurements, each of which was taken with an exposure time of 10 seconds for each direction of

the magnetization. The asymmetry of the  $3k+1$  and  $3k-1$  harmonics exhibit opposite signs - proving that the helicity of the  $3k+1$  harmonics is indeed opposite to the  $3k-1$  harmonics.

Finally, we used the measured XMCD asymmetry to extract the magneto-optical (MO) dichroic absorption coefficient  $\Delta\beta$  for Cobalt. The MO dichroic absorption coefficient is given by  $\Delta\beta = \tanh^{-1}(A) / (2|\vec{k}_0| \cos \theta L)$ , where  $\vec{k}_0$  is the light wavevector,  $L$  is the sample effective thickness and  $\theta$  is the angle between the sample magnetization and beam propagation direction [51]. Since the sample and the magnetization are tilted by  $45^\circ$ , the optical path is  $\sqrt{2}L$ , and  $\cos \theta = 1/\sqrt{2}$ , the MO dichroic coefficient is simply  $\Delta\beta = \tanh^{-1}(A) / (2|\vec{k}_0| \cdot 100nm)$ . Our results for  $\Delta\beta$  are presented in Fig. 3c. The MO coefficient measured by the left circularly polarized  $3k+1$  harmonics matches measurements that were taken using synchrotrons [54], indicating that their polarization is circular. However, the low intensity and low MO dichroic absorption coefficient measured using the right circularly polarized harmonics 29<sup>th</sup>, 32<sup>nd</sup> and 35<sup>th</sup> (corresponding to the  $3k-1$  group) at 45 eV, 50 eV and 55 eV, respectively, indicate that their polarization is elliptical and not fully circular. The reasons for the reduced circularity of the  $3k-1$  as opposed to the  $3k+1$  harmonics is not yet clear and a subject of continued investigation.

## Conclusions and outlook

We demonstrated the first bright source of circularly-polarized high harmonics and apply it for magnetic circular dichroism measurements of magnetic materials. Our HHG source produces a broad spectrum of bright circularly-polarized harmonics, where consecutive harmonics exhibit opposite helicity. This work removes a major constraint to date - that the polarization of bright high harmonics sources was limited to linear polarization. This work therefore paves the way for the studies of ultrafast circular dichroism of magnetic samples, chiral molecules and nanostructures. In combination with coherent diffraction imaging techniques, this advance will enable ultrafast dynamics imaging of magnetic domains. Our source can also be used for seeding x-ray lasers to obtain ultra-bright circularly-polarized x-rays [55]. Finally, the scheme we use is universal, and can be used to generate circularly-polarized high harmonics across broad spectral regions, for example, through quasi phase matching of the HHG process, by using mid-IR pumps [18] or by using other nonlinear media.

## Acknowledgements

This work was supported by the USA–Israel Binational Science Foundation (BSF). The Technion group is part of the Israeli Center of Research Excellence ‘Circle of Light’ supported by the I-CORE Program of the Planning and Budgeting Committee and The Israel Science Foundation. The JILA group gratefully acknowledges funding from the U.S. Department of Energy Office of Basic Energy Sciences, Award #DE-SC0002002 and from the Deutsche Forschungsgemeinschaft #GR 4234/1-1. JILA also gratefully acknowledges support from an AFOSR DURIP award for the laser system used for this work.

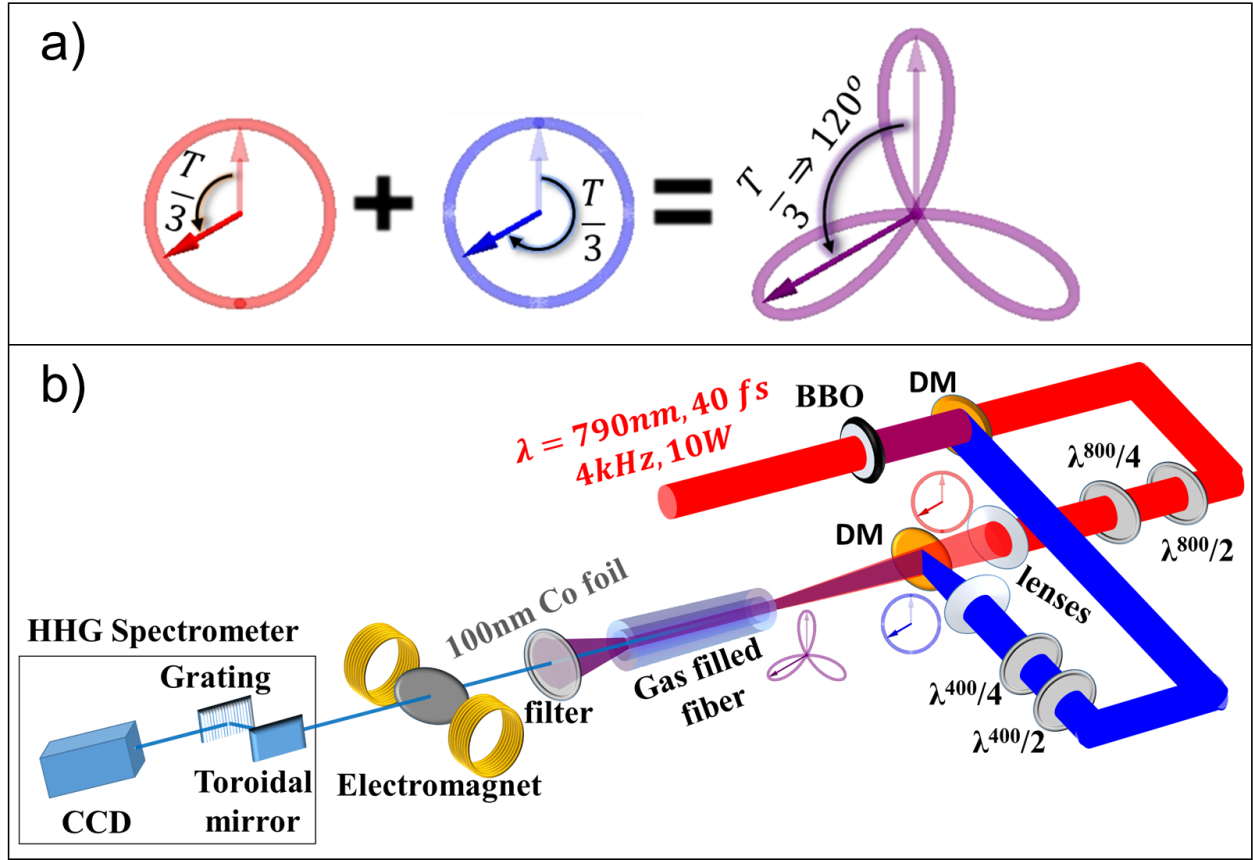


**Figure 1 | Setup for circularly-polarized HHG.** (a) The combined field of a circularly polarized 790 nm laser (red) and a counter rotating second harmonic field (blue) is a three-fold cloverleaf shape (purple). The system possess a discrete rotation dynamical symmetry of the light field, where a delay of  $T/3$  acts as a  $120^\circ$  rotation. While the plot shows the case of equal field amplitudes, the dynamical symmetry is independent of the amplitude ratio between the two fields. This dynamical symmetry gives rise to circularly polarized harmonics where harmonic orders  $q=3k+1$  rotate right, while  $q=3k+2$  rotate left (see text). (b) Schematic of the apparatus. Circular harmonics are generated by focusing the fundamental and second harmonic (with opposing helicities) into a gas filled fiber. The polarization states of the two drivers can be independently adjusted using a Mach-Zehnder setup, thereby controlling the helicity of the generated harmonics. The magnetic state of the sample foils can be probed with element-selectively by exploiting XMCD at the  $M$  absorption edge of Cobalt.

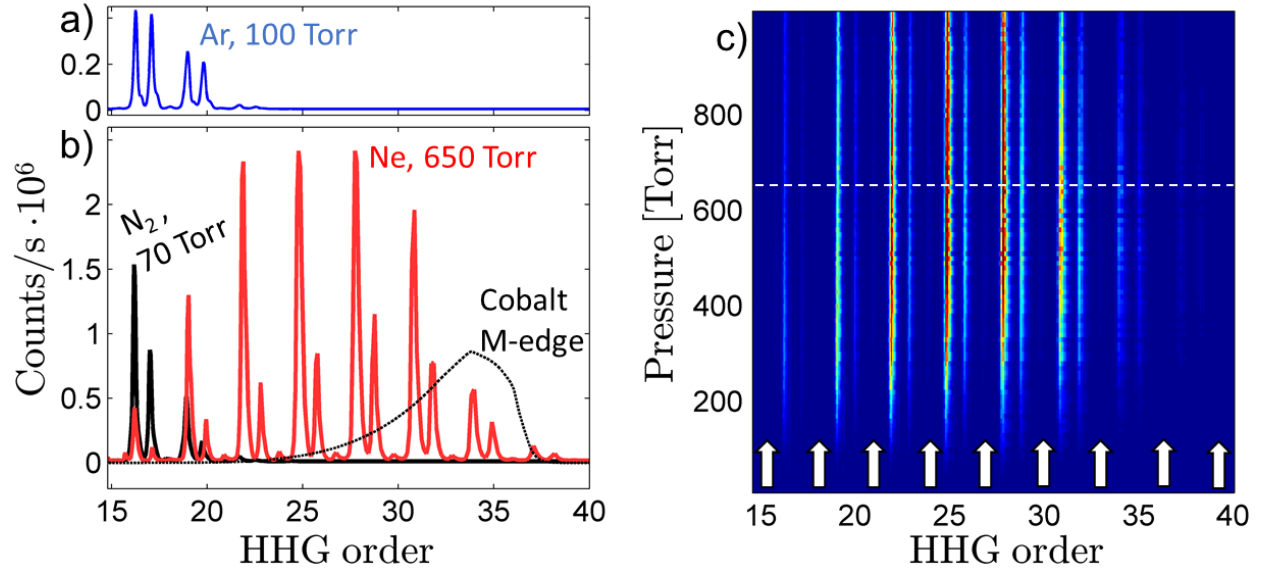


**Figure 2 | Generation of bright circularly-polarized harmonics.** (a) High harmonic spectrum using Argon and ~800 nm thick Aluminum filter. (b) Harmonic spectrum using molecular Nitrogen at 70 Torr (black) and Neon at 650 Torr (red solid curve) and 400 nm thick Aluminum filter, spanning into the Cobalt M absorption edge (black dash curve). The circular polarization of the spectrum is manifested by the suppression of the  $3k$  harmonics (15, 18, 21.... see white arrows). (c) Color coded magnitude of the generated harmonics as a function of the harmonic order and gas pressure for a waveguide filled with Neon. White dashed line at 650 Torr marks the optimal pressure.



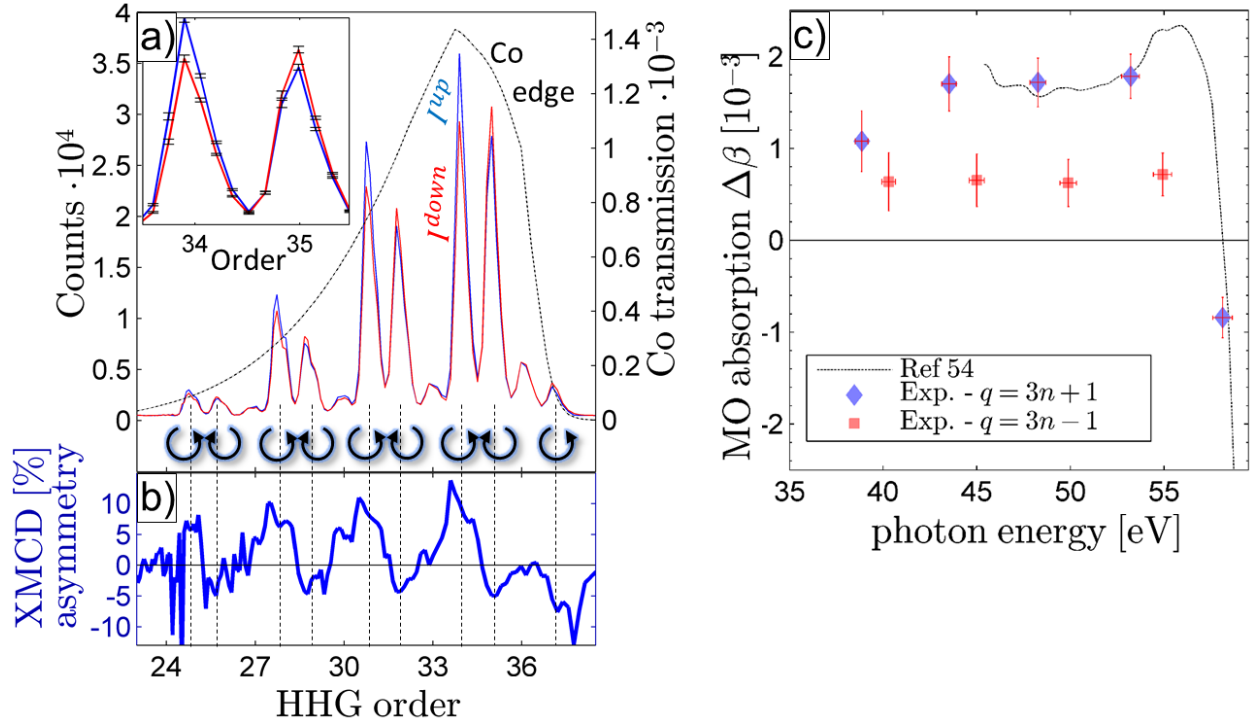


**Figure 3 | XMCD of Cobalt.** (a) Spectra of circularly polarized harmonics transmitted through 100 nm of magnetized Cobalt with magnetization direction either “up” ( $I^{\text{up}}$ , blue) and “down” ( $I^{\text{down}}$ , red). The dashed black envelope (right axis) shows the transmission spectrum of Cobalt. The inset shows the difference in signal between “up” and “down” magnetization for the 34<sup>th</sup> and 35<sup>th</sup> orders, including the experimental error. The harmonic helicity is indicated by circular arrows below each harmonic. (b) Experimental XMCD asymmetry defined by  $(I^{\text{up}} - I^{\text{down}})/(I^{\text{up}} + I^{\text{down}})$ , reaching values of 10% at the 34<sup>th</sup> harmonic, and clearly showing inverted helicity of adjacent harmonic orders. (c) Magneto-optical (MO) absorption coefficient,  $\Delta\beta$ , derived from XMCD asymmetry of the  $3k+1$  (diamonds) and  $3k-1$  (squares) harmonics. We estimate  $\Delta\beta$  from a weighted average over a harmonic peak, where the error bars are the standard deviation across the same harmonic. For comparison to previously measured values, the measured MO dichroic absorption coefficient from Ref [54] are given in the dashed line. The MO coefficients measured by the  $3k+1$  harmonics match well to Ref [54], indicating that these harmonics are indeed circularly polarized. The reduced intensities and MO coefficients of the  $3k-1$  harmonics suggests that the polarization of these harmonics is elliptical and not completely circular.

## Bibliography

- [1] N. Böwering, T. Lischke, B. Schmidtke, N. Müller, T. Khalil, and U. Heinzmann, *Phys. Rev. Lett.* **86**, 1187 (2001).
- [2] O. Travnikova, J.-C. Liu, A. Lindblad, C. Nicolas, J. Söderström, V. Kimberg, F. Gel'mukhanov, and C. Miron, *Phys. Rev. Lett.* **105**, 233001 (2010).
- [3] C. Hwang, C.-H. Park, D. A. Siegel, A. V. Fedorov, S. G. Louie, and A. Lanzara, *Phys. Rev. B* **84**, 125422 (2011).
- [4] I. Gierz, M. Lindroos, H. Höchst, C. R. Ast, and K. Kern, *Nano Lett.* **12**, 3900 (2012).
- [5] S.-Y. Xu, M. Neupane, C. Liu, D. Zhang, A. Richardella, L. Andrew Wray, N. Alidoust, M. Leandersson, T. Balasubramanian, J. Sánchez-Barriga, O. Rader, G. Landolt, B. Slomski, J. Hugo Dil, J. Osterwalder, T.-R. Chang, H.-T. Jeng, H. Lin, A. Bansil, N. Samarth, and M. Zahid Hasan, *Nat. Phys.* **8**, 616 (2012).
- [6] Y. Liu, G. Bian, T. Miller, and T.-C. Chiang, *Phys. Rev. Lett.* **107**, 166803 (2011).
- [7] G. Schütz, M. Knülle, and H. Ebert, *Phys. Scr.* **1993**, 302 (1993).
- [8] J. Stohr, J. Wu, B. D. Hermsmeier, M. G. Samant, G. R. Harp, S. Koranda, D. Dunham, and B. P. Tonner, *Science* **259**, 658 (1993).
- [9] P. Fischer, T. Eimüller, G. Schütz, G. Schmahl, P. Guttman, and G. Bayreuther, *J. Magn. Magn. Mater.* **198–199**, 624 (1999).
- [10] S. Eisebitt, J. Lüning, W. F. Schlotter, M. Lörger, O. Hellwig, W. Eberhardt, and J. Stöhr, *Nature* **432**, 885 (2004).
- [11] C. Stamm, T. Kachel, N. Pontius, R. Mitzner, T. Quast, K. Holldack, S. Khan, C. Lupulescu, E. F. Aziz, M. Wietstruk, H. A. Dürr, and W. Eberhardt, *Nat. Mater.* **6**, 740 (2007).
- [12] C. Stamm, N. Pontius, T. Kachel, M. Wietstruk, and H. A. Dürr, *Phys. Rev. B* **81**, 104425 (2010).

- [13] M. Wietstruk, A. Melnikov, C. Stamm, T. Kachel, N. Pontius, M. Sultan, C. Gahl, M. Weinelt, H. A. Dürr, and U. Bovensiepen, *Phys. Rev. Lett.* **106**, 127401 (2011).
- [14] I. Radu, K. Vahaplar, C. Stamm, T. Kachel, N. Pontius, H. A. Dürr, T. A. Ostler, J. Barker, R. F. L. Evans, R. W. Chantrell, A. Tsukamoto, A. Itoh, A. Kirilyuk, T. Rasing, and A. V. Kimel, *Nature* **472**, 205 (2011).
- [15] V. López-Flores, J. Arabski, C. Stamm, V. Halté, N. Pontius, E. Beaurepaire, and C. Boeglin, *Phys. Rev. B* **86**, 014424 (2012).
- [16] B. Pfau, S. Schaffert, L. Müller, C. Gutt, A. Al-Shemmary, F. Büttner, R. Delaunay, S. Düsterer, S. Flewett, R. Frömter, J. Geilhufe, E. Guehrs, C. M. Günther, R. Hawaldar, M. Hille, N. Jaouen, A. Kobs, K. Li, J. Mohanty, H. Redlin, W. F. Schlotter, D. Stickler, R. Treusch, B. Vodungbo, M. Kläui, H. P. Oepen, J. Lüning, G. Grübel, and S. Eisebitt, *Nat. Commun.* **3**, 1100 (2012).
- [17] C. E. Graves, A. H. Reid, T. Wang, B. Wu, S. de Jong, K. Vahaplar, I. Radu, D. P. Bernstein, M. Messerschmidt, L. Müller, R. Coffee, M. Bionta, S. W. Epp, R. Hartmann, N. Kimmel, G. Hauser, A. Hartmann, P. Holl, H. Gorke, J. H. Mentink, A. Tsukamoto, A. Fognini, J. J. Turner, W. F. Schlotter, D. Rolles, H. Soltau, L. Strüder, Y. Acremann, A. V. Kimel, A. Kirilyuk, T. Rasing, J. Stöhr, A. O. Scherz, and H. A. Dürr, *Nat. Mater.* **12**, 293 (2013).
- [18] T. Popmintchev, M.-C. Chen, D. Popmintchev, P. Arpin, S. Brown, S. Ališauskas, G. Andriukaitis, T. Balčiunas, O. D. Mücke, A. Pugzlys, A. Baltuška, B. Shim, S. E. Schrauth, A. Gaeta, C. Hernández-García, L. Plaja, A. Becker, A. Jaron-Becker, M. M. Murnane, and H. C. Kapteyn, *Science* **336**, 1287 (2012).

- [19] M. D. Seaberg, D. E. Adams, E. L. Townsend, D. A. Raymondson, W. F. Schlotter, Y. Liu, C. S. Menoni, L. Rong, C.-C. Chen, J. Miao, H. C. Kapteyn, and M. M. Murnane, *Opt. Express* **19**, 22470 (2011).
- [20] E. Goulielmakis, Z.-H. Loh, A. Wirth, R. Santra, N. Rohringer, V. S. Yakovlev, S. Zharebtsov, T. Pfeifer, A. M. Azzeer, M. F. Kling, S. R. Leone, and F. Krausz, *Nature* **466**, 739 (2010).
- [21] H. J. Wörner, J. B. Bertrand, D. V. Kartashov, P. B. Corkum, and D. M. Villeneuve, *Nature* **466**, 604 (2010).
- [22] M. E. Siemens, Q. Li, R. Yang, K. A. Nelson, E. H. Anderson, M. M. Murnane, and H. C. Kapteyn, *Nat. Mater.* **9**, 26 (2010).
- [23] Q. Li, K. Hoogeboom-Pot, D. Nardi, M. M. Murnane, H. C. Kapteyn, M. E. Siemens, E. H. Anderson, O. Hellwig, E. Dobisz, B. Gurney, R. Yang, and K. A. Nelson, *Phys. Rev. B* **85**, 195431 (2012).
- [24] S. Baker, J. S. Robinson, C. A. Haworth, H. Teng, R. A. Smith, C. C. Chirilă, M. Lein, J. W. G. Tisch, and J. P. Marangos, *Science* **312**, 424 (2006).
- [25] A. L. Cavalieri, N. Müller, T. Uphues, V. S. Yakovlev, A. Baltuška, B. Horvath, B. Schmidt, L. Blümel, R. Holzwarth, S. Hendel, M. Drescher, U. Kleineberg, P. M. Echenique, R. Kienberger, F. Krausz, and U. Heinzmann, *Nature* **449**, 1029 (2007).
- [26] P. Salières, L. Le Déroff, T. Auguste, P. Monot, P. d' Oliveira, D. Campo, J.-F. Hergott, H. Merdji, and B. Carré, *Phys. Rev. Lett.* **83**, 5483 (1999).
- [27] C. La-O-Vorakiat, M. Siemens, M. M. Murnane, H. C. Kapteyn, S. Mathias, M. Aeschlimann, P. Grychtol, R. Adam, C. M. Schneider, J. M. Shaw, H. Nembach, and T. J. Silva, *Phys. Rev. Lett.* **103**, 257402 (2009).

- [28] C. La-O-Vorakiat, E. Turgut, C. A. Teale, H. C. Kapteyn, M. M. Murnane, S. Mathias, M. Aeschlimann, C. M. Schneider, J. M. Shaw, H. T. Nembach, and T. J. Silva, *Phys. Rev. X* **2**, 011005 (2012).
- [29] S. Mathias, C. La-O-Vorakiat, P. Grychtol, P. Granitzka, E. Turgut, J. M. Shaw, R. Adam, H. T. Nembach, M. E. Siemens, S. Eich, C. M. Schneider, T. J. Silva, M. Aeschlimann, M. M. Murnane, and H. C. Kapteyn, *Proc. Natl. Acad. Sci.* (2012).
- [30] D. Rudolf, C. La-O-Vorakiat, M. Battiato, R. Adam, J. M. Shaw, E. Turgut, P. Maldonado, S. Mathias, P. Grychtol, H. T. Nembach, T. J. Silva, M. Aeschlimann, H. C. Kapteyn, M. M. Murnane, C. M. Schneider, and P. M. Oppeneer, *Nat. Commun.* **3**, 1037 (2012).
- [31] E. Turgut, C. La-o -vorakiat, J. M. Shaw, P. Grychtol, H. T. Nembach, D. Rudolf, R. Adam, M. Aeschlimann, C. M. Schneider, T. J. Silva, M. M. Murnane, H. C. Kapteyn, and S. Mathias, *Phys. Rev. Lett.* **110**, 197201 (2013).
- [32] P. B. Corkum, *Phys. Rev. Lett.* **71**, 1994 (1993).
- [33] M. Lewenstein, P. Balcou, M. Y. Ivanov, A. L’Huillier, and P. B. Corkum, *Phys. Rev. A* **49**, 2117 (1994).
- [34] P. Dietrich, N. H. Burnett, M. Ivanov, and P. B. Corkum, *Phys. Rev. A* **50**, R3585 (1994).
- [35] M. Möller, Y. Cheng, S. D. Khan, B. Zhao, K. Zhao, M. Chini, G. G. Paulus, and Z. Chang, *Phys. Rev. A* **86**, 011401 (2012).
- [36] F. A. Weihe, S. K. Dutta, G. Korn, D. Du, P. H. Bucksbaum, and P. L. Shkolnikov, *Phys. Rev. A* **51**, R3433 (1995).
- [37] V. V. Strelkov, A. A. Gonoskov, I. A. Gonoskov, and M. Y. Ryabikin, *Phys. Rev. Lett.* **107**, 043902 (2011).
- [38] O. E. Alon, V. Averbukh, and N. Moiseyev, *Phys. Rev. Lett.* **80**, 3743 (1998).

- [39] X.-M. Tong and S.-I. Chu, Phys. Rev. A **58**, R2656 (1998).
- [40] K. Nobusada and K. Yabana, Phys. Rev. A **75**, 032518 (2007).
- [41] K.-J. Yuan and A. D. Bandrauk, Phys. Rev. A **84**, 023410 (2011).
- [42] K.-J. Yuan and A. D. Bandrauk, Phys. Rev. A **83**, 063422 (2011).
- [43] A. Husakou, F. Kelkensberg, J. Herrmann, and M. J. J. Vrakking, Opt. Express **19**, 25346 (2011).
- [44] B. Vodungbo, A. Barszczak Sardinha, J. Gautier, G. Lambert, C. Valentin, M. Lozano, G. Iaquaniello, F. Delmotte, S. Sebban, J. Luning, and P. Zeitoun, Opt. Express **19**, 4346 (2011).
- [45] L. Z. Liu, K. O’Keeffe, and S. M. Hooker, Opt. Lett. **37**, 2415 (2012).
- [46] A. Fleischer, P. Sidorenko, and O. Cohen, Opt. Lett. **38**, 223 (2013).
- [47] K.-J. Yuan and A. D. Bandrauk, Phys. Rev. Lett. **110**, 023003 (2013).
- [48] S. Long, W. Becker, and J. K. McIver, Phys. Rev. A **52**, 2262 (1995).
- [49] H. Eichmann, A. Egbert, S. Nolte, C. Momma, B. Wellegehausen, W. Becker, S. Long, and J. K. McIver, Phys. Rev. A **51**, R3414 (1995).
- [50] A. Fleischer, O. Kfir, T. Diskin, P. Sidorenko, and O. Cohen, *Does High Harmonic Generation Conserve Angular Momentum?* (2013).
- [51] P. M. Oppeneer, *Handbook of Magnetic Materials in Vol.13 Pp. 229* (Elsevier, 2001).
- [52] A. Rundquist, C. G. Durfee, Z. Chang, C. Herne, S. Backus, M. M. Murnane, and H. C. Kapteyn, Science **280**, 1412 (1998).
- [53] T. Popmintchev, M.-C. Chen, A. Bahabad, M. Gerrity, P. Sidorenko, O. Cohen, I. P. Christov, M. M. Murnane, and H. C. Kapteyn, Proc. Natl. Acad. Sci. **106**, 10516 (2009).
- [54] S. Valencia, A. Gaupp, W. Gudat, H.-C. Mertins, P. M. Oppeneer, D. Abramsohn, and C. M. Schneider, New J. Phys. **8**, 254 (2006).

- [55] P. Zeitoun, G. Faivre, S. Sebban, T. Mocek, A. Hallou, M. Fajardo, D. Aubert, P. Balcou, F. Burgy, D. Douillet, S. Kazamias, G. de Lachèze-Murel, T. Lefrou, S. le Pape, P. Mercère, H. Merdji, A. S. Morlens, J. P. Rousseau, and C. Valentin, *Nature* **431**, 426 (2004).